Xu et al. Nanoscale Research Letters (2018) 13:65
https://doi.org/10.1186/s11671-018-2469-6

Nanoscale Research Letters

NANO EXPRESS Open Access

3D Interconnected V_6O_{13} Nanosheets Grown on Carbonized Textile via a Seed-Assisted Hydrothermal Process as High-Performance Flexible Cathodes for Lithium-Ion Batteries

Shixing Xu[1], Dingcheng Cen[1], Peibo Gao[1], Huang Tang[2*] and Zhihao Bao[1*]

Abstract

Three-dimensional (3D) free-standing nanostructured materials have been proven to be one of the most promising electrodes for energy storage due to their enhanced electrochemical performance. And they are also widely studied for the wearable energy storage systems. In this work, interconnected V_6O_{13} nanosheets were grown on the flexible carbonized textile (c-textile) via a seed-assisted hydrothermal method to form a 3D free-standing electrode for lithium-ion batteries (LIBs). The electrode exhibited a specific capacity of 170 mA h g^{-1} at a specific current of 300 mA g^{-1}. With carbon nanotube (CNT) coating, its specific capacities further increased 12–40% at the various current rates. It could retain a reversible capacity of 130 mA h g^{-1}, 74% of the initial capacity after 300 cycles at the specific current of 300 mA g^{-1}. It outperformed most of the mixed-valence vanadium oxides. The improved electrochemical performance was ascribed to the synergistic effect of the 3D nanostructure of V_6O_{13} for feasible Li^+ diffusion and transport and highly conductive hierarchical conductive network formed by CNT and carbon fiber in c-textile.

Keywords: Interconnected V_6O_{13} nanosheets, Seed-assisted hydrothermal, Lithium-ion batteries

Background

Vanadium oxides (e.g., V_6O_{13}, V_3O_7, V_2O_5) are cathode materials applicable for high-energy lithium-ion battery (LIB), due to their low cost, high specific capacities, and the abundance of vanadium element [1–6]. Among the oxides, V_6O_{13} has been considered as an excellent candidate of the cathode material [7–14]. Its theoretical capacity and energy density can reach 417 mA h g^{-1} and 890 Wh kg^{-1} when lithiated to the final product, $Li_8V_6O_{13}$ [2, 8]. However, V_6O_{13} electrodes have suffered short cycle life and low rate capability for a long time because V_6O_{13}'s electronic conductivity decreases when lithiated while Li^+ diffusion coefficients (10^{-8} to 10^{-9} cm^2 S^{-1}) are low [7, 9]. Constructing free-standing 3D nanostructures is an effective method to solve the above problems. 3D nanostructure can enhance ion/electron transport/diffusion while effectively avoids self-aggregation [15–20]. For example, Yu et al. synthesized 3D V_6O_{13} nanotextiles assembled from interconnected nanogrooves via a facile solution-redox-based self-assembly route with MnO_2 template at room temperature. In a voltage range of 1–4 V, V_6O_{13} nanotextiles exhibited reversible capacities of 326 and 134 mA h g^{-1} at 20 and 500 mA g^{-1}, respectively, and a capacity retention of above 80% after 100 cycles at 500 mA g^{-1} [2]. Tong et al. fabricated V_6O_{13} cathode supported by a steel mesh with wrinkles by the similar route. The free-standing electrode with a loading amount of V_6O_{13} up to 2.0 mg cm^{-2} was obtained. At a current density of 500 mA g^{-1}, the V_6O_{13} electrode demonstrated an initial capacity of 225 mA h g^{-1} that deteriorated to around

* Correspondence: tangh@126.com; zbao@tongji.edu.cn
[2]School of Mathematics and Physics, Jiangsu University of Technology, 1801 Zhongwu Road, Changzhou 213001, China
[1]Shanghai Key Laboratory of Special Artificial Microstructure Materials and Technology, School of Physics Science and Engineering, Tongji University, 1239 Siping Road, Shanghai 200092, China

150 mA h g^{-1} after 500 cycles [21]. However, above research involved the two-step electrodeposition and removal of MnO_2. Direct growth of mixed-valence vanadium oxide nanostructure with good electrochemical property remains a great challenge [22]. Meanwhile, previous studies have not demonstrated V_6O_{13}-based flexible cathode, which has a potential use in the wearable devices.

Herein, we proposed a simple hydrothermal process to successfully grow interconnected V_6O_{13} nanosheets on the carbonized textile to fabricate a 3D free-standing electrode. It exhibited specific capacities of 161 and 105 mA h g^{-1} at the specific currents of 300 and 1200 mA h g^{-1}, respectively. With carbon nanotube (CNT) coating to further improve its conductivity, its specific capacities increased to 170 and 140 mA h g^{-1}. Meanwhile, its cycling performance was also improved. It could retain 74% of initial capacity with CNT coating, compared with 50% retention without CNT coating after 400 cycles at 300 mA g^{-1}. The improvement on the electrochemical performance was mainly ascribed to the synergistic effect of the 3D nanostructure of V_6O_{13} and hierarchical conductive network.

Methods

Synthesis of c-textile

The commercially available bamboo cloth was soaked in a solution with 2.5 g NaF and 60 ml H_2O for 1 h and dried for 5 h in 120 °C oven. The dried textile was carbonized at 800 °C in N_2 for 30 min to obtain c-textile.

Growth of 3D V_6O_{13} Nanostructure on c-textile

3D V_6O_{13} nanostructure was grown on c-textile by a seed-assisted hydrothermal method. c-textile was slightly oxidized in the condensed nitric acid (80 wt%) for 30 min. V_2O_5 powder (1 mg) was added to 5 ml deionized water and then ultrasonicated for 15 min to obtain a suspension. The oxidized c-textile was then immersed into the suspension for 2 h, dried, and heated at 300 °C for 10 min to grow the seed of vanadium oxide on c-textile. V_2O_5 powder (16 mg) was added to 224 μl of 30 wt% H_2O_2 and stirred for 10 min to obtain a brown solution. It was then diluted with additional 40 ml distilled water and stirred for 30 min. After the solution was transferred into a 25-ml stainless-steel autoclave, the oxidized c-textile was immersed into the solution. The autoclave was kept at 180 °C for 48 h, then the sample was washed with distilled water and alcohol and dried at 60 °C for 8 h to finally get the flexible 3D free-standing V_6O_{13} nanostructure supported with flexible c-textile. CNT was further coated on V_6O_{13} nanostructure by repeatedly dipping it into NMP suspension (0.5 mg/mL) of multi-walled CNT and drying to produce a V_6O_{13}/CNT composite electrode.

Characterization of Materials

Morphology of the product was observed by a scanning electron microscopy (SEM, Philips XL30 FEG) and a transmission electron microscopy (TEM, JEOL JEM-2010). X-ray photoelectron spectroscopy (XPS) analyses (K-Alpha) were performed using a monochromatic Al Ka source.

Battery Fabrication and Electrochemical Measurements

Standard CR2016-type coin cells were assembled in an argon-filled glove box (Vigor Inc. Suzhou, China) with V_6O_{13} electrode as the working electrode with a mass loading of ~ 1 mg cm^{-2}. A lithium foil was used as the counter electrode; 1 mol $LiPF_6$ in a mixture of ethylene carbonate (EC), diethyl carbonate (DEC), and dimethyl carbonate (DMC) with a volume ratio of 1:1:1 was used as the electrolyte, and a polypropylene film was used as the separator. The assembled cells were electrochemically cycled between 1.5 and 4.0 V vs. Li/Li^+ for galvanostatic charge/discharge on a LAND battery test system (Wuhan Kingnuo Electronics Co., Ltd., China) at 25 °C. Electrochemical impedance spectroscopy (EIS) studies were conducted with Autolab PGSTAT302N workstation in the frequency range of 10 mHz to 10 kHz.

Results and Discussion

The schematic of the growth of 3D V_6O_{13} interconnected nanosheets on c-textile was shown in Additional file 1: Figure S1. The textile (Fig. 1a) was firstly carbonized at 800 °C to obtain c-textile (Fig. 1b). SEM images (Fig. 2a) showed that c-textile was composed of weaved bundles of carbon fibers with a diameter of ~ 5 μm. c-textile exhibited excellent flexibility and mechanical strength. It was able to be rolled and twisted as shown in Fig. 1c. The square resistivity of the c-textile was measured to be 5 Ω/sq. with the four-probe method. Thus, it was used as a promising flexible support/collector for the electrode materials. It was then immersed in VO_x suspension, dried, and kept at 300 °C for 10 min to grow the seed crystals. Its weight change was undetectable (< 0.1 mg). After being immersed in vanadium oxide (VO_x) sol solution for the hydrothermal growth, the black c-textile was covered with a layer of a yellow-green thin film; however, its flexibility was kept, as shown in Fig. 1d. Its resistivity increased to 50 Ω/sq. SEM images (Fig. 2b, c) further showed that it was composed of several micron-long and several hundred nanometer-wide interconnected nanosheets, as building blocks to construct 3D nanostructure on c-textile. High-resolution TEM image (Fig. 2f) showed well-defined lattice fringes of the grown nanosheets. The spacing of 3.5 Å in the lattice fringe was consistent with (110) interplanar distance of the orthogonal V_6O_{13} phase (PDF card No.71-2235) which was in agreement with the XRD

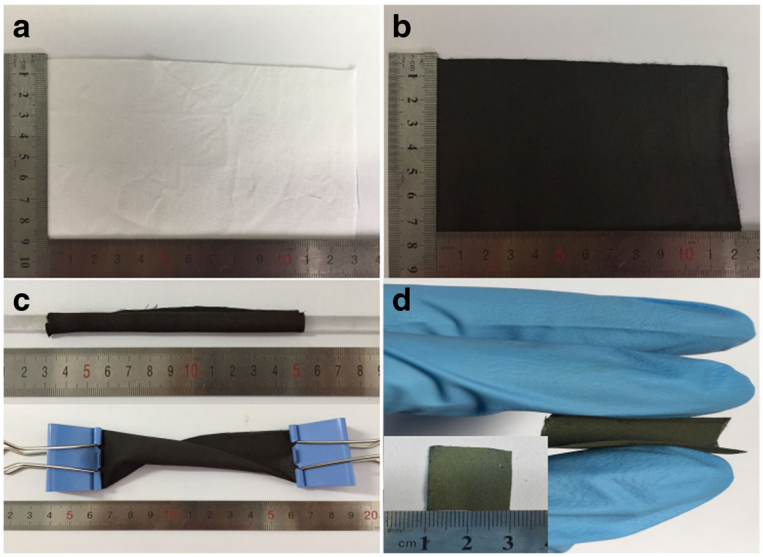

Fig. 1 Optical images of **a** commercially available textile, **b** carbonized textile, **c** rolled and twisted c-textile, and **d** c-textile with grown V_6O_{13} at the rolled state, inset: at the flat state

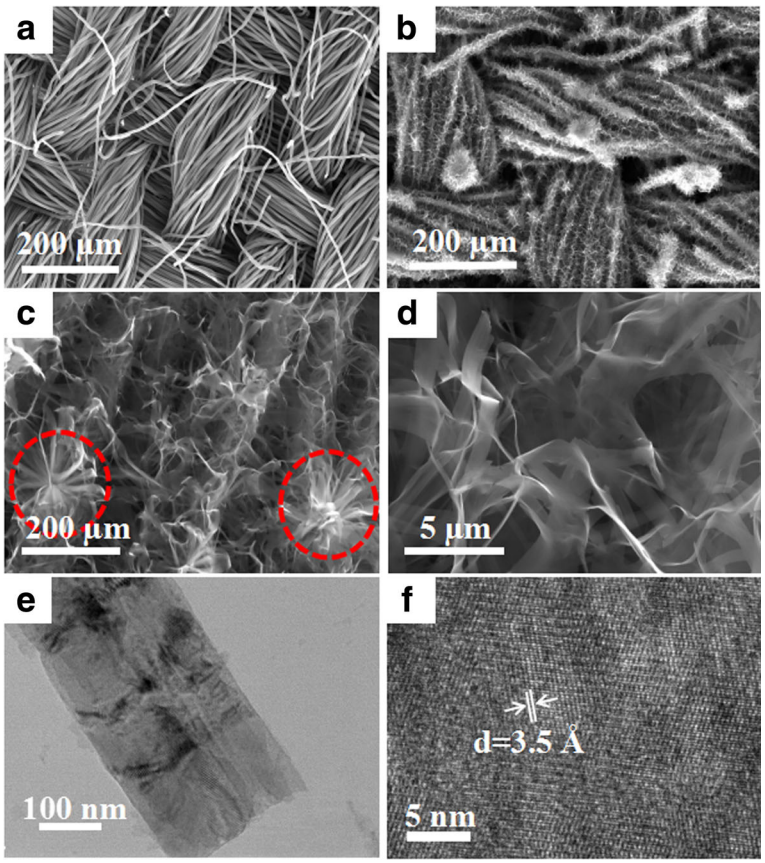

Fig. 2 Microstructure of 3D free-standing interconnected V_6O_{13} nanosheets on c-textile: **a**, **b** low resolution SEM images of c-textile without and with nanosheets, respectively; **c**, **d** high-resolution SEM images of interconnected nanosheets grown on c-textile; **e**, **f** low- and high-resolution TEM images of the nanosheet, respectively

pattern (Fig. 3c). The growth mechanism was that seed crystal firstly nucleated on the sites with an oxygen-bearing functional group [23, 24]. Then during the hydrothermal process in the VO_x aqueous solution, interconnected V_6O_{13} nanosheets were continuously grown on the seed crystals. As for the formation of 3D structured microflowers, it might be due to the several seed crystals aggregated at the same location for growth of the nanosheets. To further determine the valence state of vanadium element in V_6O_{13}, XPS analyses were conducted on the synthesized interconnected V_6O_{13} nanosheets. The survey XPS scan (Fig. 3a) revealed that the sample was composed of V, O, C, and N elements. The binding energies for vanadium 2p3/2 and 2p1/2 were identified in Fig. 3b at 516.0 and 523.9 eV for V^{4+} and 517.3 and 525.0 eV for V^{5+}, respectively. It was well consistent with the chemical state of vanadium in V_6O_{13} reported [25–27]. The above results confirmed that 3D V_6O_{13} nanostructures were successfully grown on c-textile via a simple seed-assisted hydrothermal process.

To investigate the electrochemical performance of 3D V_6O_{13} nanostructures grown on c-textile, half-cell coin batteries were assembled with a V_6O_{13} electrode as the cathode and lithium foil as the anode. Figure 4a displayed typical cyclic voltammetry (CV) curves of V_6O_{13} electrode in a scan rate of 0.2 mV s^{-1} between 1.5 and 4.0 V (vs. Li/Li^+). The main redox peaks at 2.8/2.5 V could be easily identified. Broad anodic peak at ~ 3.2 and 2.3 V and cathodic peak at ~ 1.8 V could also be observed [11, 28]. The appearance of the above peaks indicated multi-step phase transitions, and the location of peak voltages was consistent with the previously reported ones [2]. Figure 4b showed the galvanostatic discharge/charge curve for the first cycle at the specific current of 30 mA g^{-1}. Multiple poorly defined voltage plateaus could be identified. In the discharge curve, two sloped plateaus were identified at 2.3 and 2.8 V, corresponding to the anodic peaks. When the specific currents increased from 30 to 150, 300, 600, and 1200 mA g^{-1}, the specific capacities were 253, 176, 161, 133, and 105 mA h g^{-1}. The good electrochemical properties were due to the 3D nanostructure composed of V_6O_{13} nanosheets. Such open structure could contact with electrolytes very well and shorten the Li^+ transport and diffusion path. The morphology of the original V_6O_{13} electrode and the cycled electrode with SEI was examined under SEM (Additional file 1: Figure S2). The morphology of 3D interconnected nanosheets was retained during the cycling. This further suggests the importance of the 3D nanostructure on the structural integrity of V_6O_{13} electrode during the electrochemical cycling. However, the conductivity of V_6O_{13} decreased as lithiation proceeded [7, 29]. Moreover, the length of nanosheet in the V_6O_{13} electrode reached several tens of microns. Only a small portion of individual nanosheet is directly connected with the conductive carbon fibers of c-textile, which served as the collector. It could hinder the electron transfer during the charge/discharge process. To further enhance the conductivity, and thus the electrochemical properties of the 3D free-standing V_6O_{13} electrode, it was immersed in

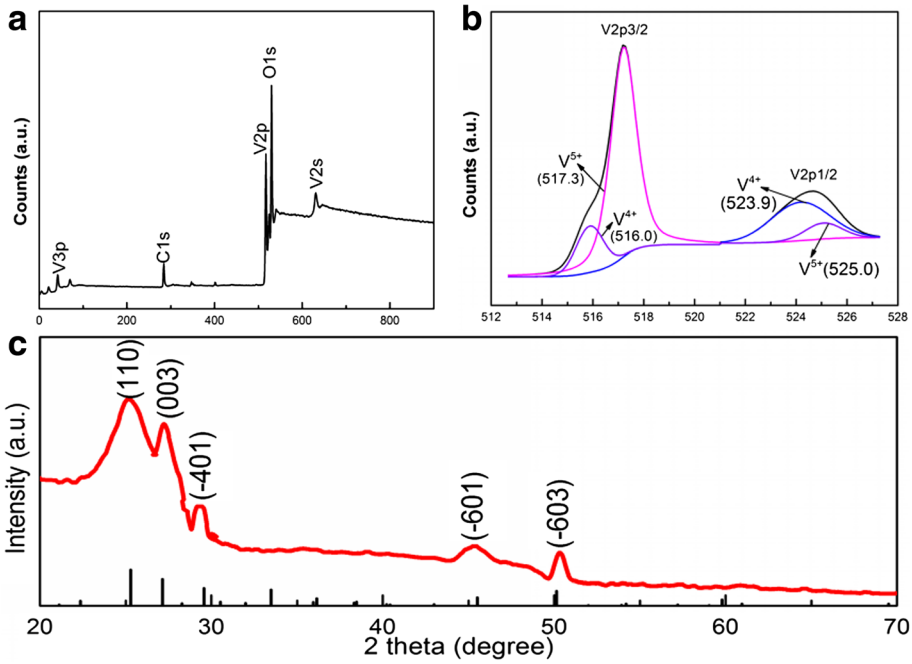

Fig. 3 **a** A survey XPS spectrum of 3D free-standing interconnected V_6O_{13} nanosheets grown on c-textile. **b** Spectrum of V_{2p} and O_{1s} with a fitted curve. **c** The XRD patterns of V_6O_{13}

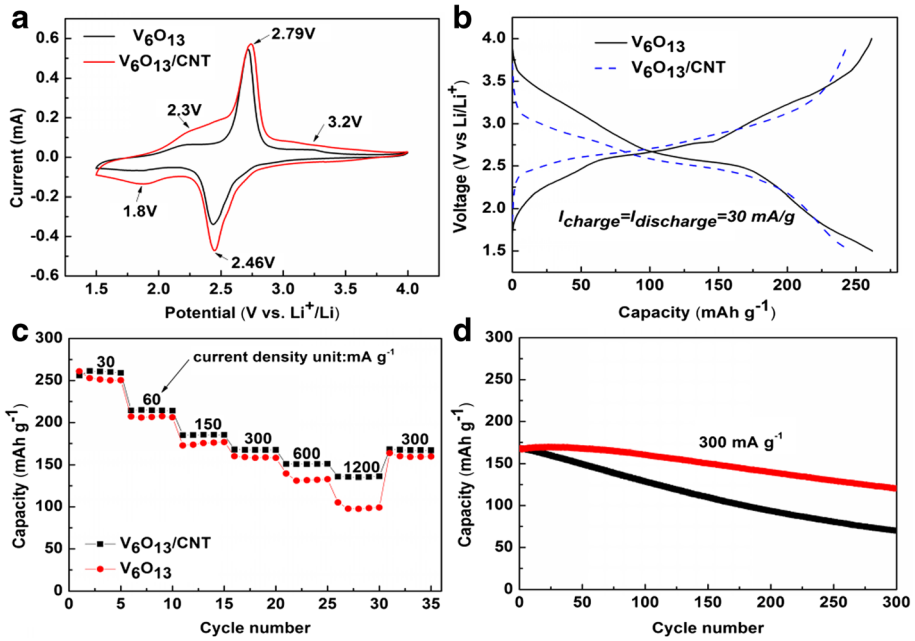

Fig. 4 Electrochemical performance of 3D free-standing V_6O_{13} electrodes with/without CNT coating. **a** Cyclic voltammetry curves. **b** Galvanostatic charge/discharge curves. **c** Rate. **d** Cyclability performance of the two electrodes

CNT dispersion to dip-coat CNT on its surface. Figure 5a, b showed SEM images of the V_6O_{13} electrode with CNT. CNT was successfully deposited in the plane of V_6O_{13} nanosheets and intimately contacted with them. Even the bridging was built through CNTs between neighboring nanosheets, as shown in Fig. 5c. As expected, the resistivity of the V_6O_{13} electrode with CNT decreased from 50 to 20 Ω/sq. After the coating of CNTs, the redox peak appeared at the same position on CV profile (Fig. 4a) while peak currents increased. It indicated fast kinetic of electrochemical reaction in V_6O_{13} electrode with CNT. The V_6O_{13} electrode with CNT exhibited better rate performance compared with the electrode without CNT coating, as shown in Fig. 4c. The specific discharge capacities were 261, 185, 170, 153, and 140 mA h g^{-1} at the specific currents of 30, 150, 300, 600, and 1200 mA g^{-1}, respectively, corresponding to 12~40% increase compared with the composite cathode without CNTs. To further verify the role of CNT, we calculated the lithium ion diffusion coefficient with cyclic voltammetry. The V_6O_{13}/CNT anodic and cathodic diffusion coefficients were 4.79×10^{-8} and 2.01×10^{-8} cm^2 s^{-1}, higher than V_6O_{13} electrode's 2.42×10^{-8} and 1.7×10^{-8} cm^2 s^{-1}, respectively (and the associated discussion is in Additional file 1: Figure S3). Nyquist plots (Fig. 6a) of V_6O_{13} electrode and V_6O_{13} electrode with CNT displayed similar shapes, a semicircle shape in the high-to-medium frequency domain and an inclined line in the low-frequency regions, corresponding to electrochemical reaction impedance (charge transfer process) and diffusion process of lithium ions. The inset is the equivalent circuit used to fit Nyquist plots. In the circuit, CPE is the constant phase angle element and W is the Warburg impedance. R_s and R_{ct} represent the ohmic resistance (total resistance of the electrolyte, separator, and

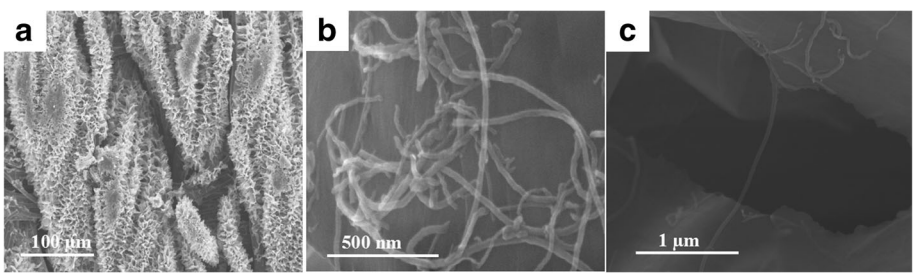

Fig. 5 Microstructure of CNT-coated V_6O_{13} electrode. **a** Low-resolution SEM image of the electrode. **b**, **c** High-resolution SEM image of the electrode showing CNT covering on the nanosheet and bridging between the nanosheets

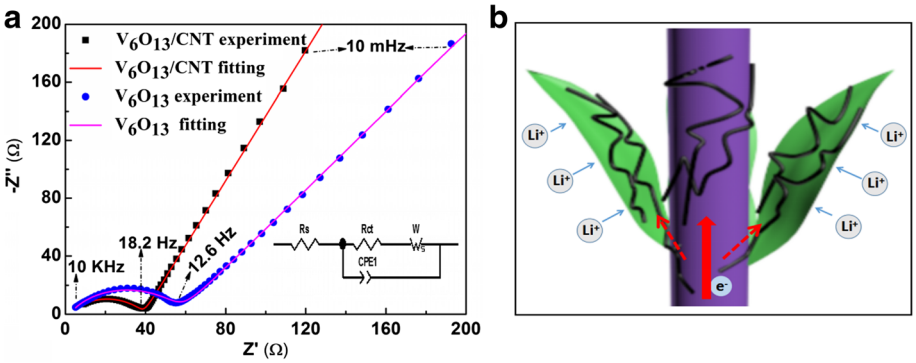

Fig. 6 **a** Nyquist plots of V_6O_{13} electrode with/without CNT coating. **b** Schematic of the transporting path for electrons in CNT-coated V_6O_{13} electrode

electrical contacts) and the charge transfer resistance, respectively [22, 30]. Additional file 1: Table S1 listed the parameters used to fit the plots. R_{ct} for the V_6O_{13}/CNT electrode was calculated to be 37.24 Ω, lower than that of V_6O_{13} (55.58 Ω). This decrease in charge transfer resistance was ascribed to the addition of CNT. The mechanism was illustrated in Fig. 6b. CNT intimately connected with V_6O_{13} nanosheets for faster electron transferring. Furthermore, CNTs and carbon fiber in the c-textile composed hierarchical conductive network for better electron conducting. The cyclability of V_6O_{13} electrodes was shown in Fig. 4d. At the specific current of 300 mA g^{-1}, the electrode with CNT coating could maintain 74% of the initial capacity of 170 mA h g^{-1} after 300 charge/discharge cycles, while the V_6O_{13} electrode only retained 42% of its initial capacity. It outperformed most of the low dimensional mixed-valence vanadium oxides or their 3D nanostructure listed in Additional file 1: Table S2. The better cyclability of V_6O_{13} electrode with CNT might be ascribed to the following reasons: (1) Reinforced with CNT, V_6O_{13}'s mechanical properties were improved. (2) Even if V_6O_{13} nanostructure was broken during the discharge/charge process, it was still attached to CNT and could be electrochemically activated. (3) Self-segregation of V_6O_{13} nanosheets was limited by the appearance of CNT. (4) CNT coating might be a valid barrier to alleviate side reaction of vanadium oxide with electrolyte, if any. Thus, CNT coating can be a facile alternative way to improve the conductivity of the 3D nanostructure, other than carbon coating and polymeric coating which usually require tremendous chemical synthesis work [14]. The overall electrochemical performance of V_6O_{13} cathode was limited by the conductivity of carbon cloth, the Li diffusivity in V_6O_{13} materials, and electron transfer between V_6O_{13} nanostructures and the carbon cloth. In the future work, further improvement can be made in the following ways: (1) reducing the resistance of the carbon cloth substrate, (2) doping V_6O_{13} with sulfur to improve its diffusivity of lithium ion, and (3) coating the V_6O_{13} with conductive polymer coating.

Conclusions

In summary, we successfully fabricated 3D free-standing V_6O_{13} nanostructure composed of interconnected nanosheets via a facile seed-assisted hydrothermal process as a cathode for LIB. The electrode exhibited good electrochemical performance. It could be further improved by coating 3D V_6O_{13} nanostructure with CNT, outperforming most of the mixed-valence vanadium oxides. Its excellent performance was due to its open 3D nanostructure and hierarchical conductive network composed of CNT in nanoscale and carbon fiber in microscale. The design of 3D nanostructure with the building block (e.g., nanowire, nanosheet) combined with constructing of the hierarchical conductive path by CNT coating can be extended to other electrode materials for better electrochemical performance.

Additional file

Additional file 1: 3D interconnected V_6O_{13} nanosheets grown on carbonized textile via a seed-assisted hydrothermal process as high-performance flexible cathodes for lithium-ion batteries. (DOCX 1386 kb)

Abbreviations

3D: Three dimensional; CE: Coulombic efficiency; CNT: Carbon nanotube; c-textile: Carbonized textile; CV: Cyclic voltammetry; DEC: Diethyl carbonate; DMC: Dimethyl carbonate; EC: Ethylene carbonate; EIS: Electrochemical impedance spectroscopy; LIB: Lithium-ion battery; SEM: Scanning electron microscopy; TEM: Transmission electron microscopy

Acknowledgments

This work was supported by NSFC-Xinjiang Jointly Key Project (No. U1503292) and Natural science Foundation of Jiangsu province, China (No. BK20171199).

Authors' contributions

HT and ZB conceived the project and supervised the study. SX conducted the material preparation, electrochemical evaluation, and structural analysis and drafted the manuscript. DC and PG helped with the electrochemical studies. All authors read and approved the final manuscript.

Competing interests
The authors declare that they have no competing interest.

Publisher's Note

Received: 26 October 2017 Accepted: 5 February 2018
Published online: 01 March 2018

References

1. Chao D, Xia X, Liu J, Fan Z, Ng CF, Lin J, Zhang H, Shen ZX, Fan HJ (2014) A V_2O_5/conductive-polymer core/shell nanobelt array on three-dimensional graphite foam: a high-rate, ultrastable, and freestanding cathode for lithium-ion batteries. Adv Mater 26:5794–5800
2. Ding YL, Wen Y, Wu C, van Aken PA, Maier J, Yu Y (2015) 3D V_6O_{13} nanotextiles assembled from interconnected nanogrooves as cathode materials for high-energy lithium ion batteries. Nano Lett 15:1388–1394
3. Li L, Liu P, Zhu K, Wang J, Liu J, Qiu J (2015) A general and simple method to synthesize well-crystallized nanostructured vanadium oxides for high performance li-ion batteries. J Mater Chem A 3:9385–9389
4. Mai L, Wei Q, An Q, Tian X, Zhao Y, Xu X, Xu L, Chang L, Zhang Q (2013) Nanoscroll buffered hybrid nanostructural VO_2 (B) cathodes for high-rate and long-life lithium storage. Adv Mater 25:2969–2973
5. Liu M, Su B, Tang Y, Jiang X, Yu A (2017) Recent advances in nanostructured vanadium oxides and composites for energy conversion. Adv Energy Mater 7:1700885
6. Chernova NA, Roppolo M, Dillon AC, Whittingham MS (2009) Layered vanadium and molybdenum oxides: batteries and electrochromics. J Mater Chem 19:2526
7. West K, Zachau-Christiansen B, Jacobsen T (1829-1833) Electrochemical properties of non-stoichiometric V_6O_{13}. Electrochim Acta 1983:28
8. Murphy DW, Christian PA (1979) Solid state electrodes for high energy batteries. Science 205:651–656
9. Murphy DW (1979) Vanadium oxide cathode materials for secondary lithium cells. J Electrochem Soc 126:497
10. Meng W, Pigliapochi R, Bayley PM, Pecher O, Gaultois MW, Seymour ID, Liang H-P, Xu W, Wiaderek KM, Chapman KW et al (2017) Unraveling the complex delithiation and lithiation mechanisms of the high capacity cathode material V_6O_{13}. Chem Mater 29:5513–5524
11. Zou Z, Cheng H, He J, Long F, Wu Y, Yan Z, Chen H (2014) V_6O_{13} nanosheets synthesized from ethanol-aqueous solutions as high energy cathode material for lithium-ion batteries. Electrochim Acta 135:175–180
12. He J, Wang W, Zou Z, Long F, Fu Z (2014) Solvothermal synthesis and electrochemical performance of rod-like V_6O_{13} as cathode material for lithium ion battery. J Electroceram 32:276–282
13. Xu N, Ma X, Wang M, Qian T, Liang J, Yang W, Wang Y, Hu J, Yan C (2016) Stationary full li-ion batteries with interlayer-expanded V_6O_{13} cathodes and lithiated graphite anodes. Electrochim Acta 203:171–177
14. Saidi M (1995) Composite cathode formulation effects on the discharge characteristics of lithium rechargeable cells based on V_6O_{13}. Solid State Ionics 78:169–173
15. Zou Z (2017) Hydrothermal synthesis of high specific capacity Al-doped V_6O_{13} cathode material for lithium-ion battery. Int J Electrochem Sci 12: 1670–1679
16. Zhang Y, Zhou M, Fan M, Huang C, Chen C, Cao Y, Li H, Liu X (2011) Improvement of the electrochemical properties of $V_3O_7{\cdot}H_2O$ nanobelts for Li battery application through synthesis of v3o7@c core-shell nanostructured composites. Curr Appl Phys 11:1159–1163
17. Liu P, Xu Y, Zhu K, Bian K, Wang J, Sun X, Gao Y, Luo H, Lu L, Liu J (2017) Ultrathin VO_2 nanosheets self-assembled into 3D micro/nano-structured hierarchical porous sponge-like micro-bundles for long-life and high-rate li-ion batteries. J Mater Chem A 5:8307–8316
18. Pan A, Wu HB, Yu L, Lou XWD (2013) Template-free synthesis of VO_2 hollow microspheres with various interiors and their conversion into V_2O_5 for lithium-ion batteries. Angew Chem 125:2282–2286
19. Lai X, Halpert JE, Wang D (2012) Recent advances in micro-/nano-structured hollow spheres for energy applications: from simple to complex systems. Energy Environ Sci 5:5604–5618
20. Wang B, Al Abdulla W, Wang D, Zhao XS (2015) A three-dimensional porous lifepo4cathode material modified with a nitrogen-doped graphene aerogel for high-power lithium ion batteries. Energy Environ Sci 8:869–875
21. Wu Z, Qiu W, Chen Y, Luo Y, Huang Y, Lei Q, Guo S, Liu P, Balogun M-S, Tong Y (2017) Etched current collector-guided creation of wrinkles in steel-mesh-supported V_6O_{13} cathode for lithium-ion batteries. J Mater Chem A 5: 756–764
22. Liu P, Zhu K, Gao Y, Luo H, Lu L (2017) Recent progress in the applications of vanadium-based oxides on energy storage: from low-dimensional nanomaterials synthesis to 3D micro/nano-structures and free-standing electrodes fabrication. Adv Energy Mater 7:1700547
23. Schmeide K, Sachs S, Bubner M, Reich T, Heise KH, Bernhard G (2003) Interaction of uranium (vi) with various modified and unmodified natural and synthetic humic substances studied by exafs and ftir spectroscopy. Inorg Chim Acta 351:133–140
24. Schwanninger M, Rodrigues JC, Pereira H, Hinterstoisser B (2004) Effects of short-time vibratory ball milling on the shape of ft-ir spectra of wood and cellulose. Vib Spectrosc 36:23–40
25. Huang Z, Zeng H, Xue L, Zhou X, Zhao Y, Lai Q (2011) Synthesis of vanadium oxide, V_6O_{13} hollow-flowers materials and their application in electrochemical supercapacitors. J Alloys Compd 509:10080–10085
26. Zhai T, Lu X, Ling Y, Yu M, Wang G, Liu T, Liang C, Tong Y, Li Y (2014) A new benchmark capacitance for supercapacitor anodes by mixed-valence sulfur-doped V_6O_{13-x}. Adv Mater 26:5869–5875
27. Wu J, Huang W, Shi Q, Cai J, Zhao D, Zhang Y, Yan J (2013) Effect of annealing temperature on thermochromic properties of vanadium dioxide thin films deposited by organic sol–gel method. Appl Surf Sci 268:556–560
28. Howing J, Gustafsson T, Thomas JO (2004) $Li_{3+\delta}V_6O_{13}$: a short-range-ordered lithium insertion mechanism. Acta crystallographica. Section B Struct Sci 60: 382–387
29. Fei H, Lin Y, Wei M (2014) Facile synthesis of V_6O_{13} micro-flowers for li-ion and na-ion battery cathodes with good cycling performance. J Colloid Interface Sci 425:1–4
30. Yu R, Zhang C, Meng Q, Chen Z, Liu H, Guo Z (2013) Facile synthesis of hierarchical networks composed of highly interconnected V_2O_5 nanosheets assembled on carbon nanotubes and their superior lithium storage properties. ACS Appl Mater Interfaces 5:12394–129.1